

Shape memory Epoxy Nanocomposites With Carbonaceous Fillers and In-Situ Generated Silver Nanoparticles

Andrea Dorigato , Alessandro Pegoretti 

Department of Industrial Engineering and INSTM Research Unit, University of Trento, Trento, Italy

Aim of this work is to develop a novel epoxy based nanocomposite and to analyse its shape memory behavior. In particular, silver nanoparticles are in-situ generated within an epoxy resin subsequently filled with both carbon black (CB) and carbon nanofibers (NFs) at different ratios and at a total amount of 4 wt%. Differential scanning calorimetry shows how the introduction of both CB and NF induces a slight decrease of the glass transition temperature (T_g) of the samples. The T_g drop due to nanofiller addition determines a decrease of both flexural modulus and stress at yield with respect to the neat resin, especially at elevated CB concentrations, while the presence of Ag nanoparticles plays a positive effect on the flexural properties. The best mechanical properties can be detected at a CF/NF ratio of 50%, coupled with a noticeable decrease of the electrical resistivity down to $10^2 \Omega\cdot\text{cm}$ and an interesting heating capability through Joule effect. The electro-mechanical shape-memory characterization under bending configuration demonstrates how it is possible to obtain an almost complete shape recovery after 60 s under an applied voltage of 220 V. POLYM. ENG. SCI., 59:694–703, 2019. © 2018 Society of Plastics Engineers

INTRODUCTION

Epoxy resins are nowadays the most widely applied matrices for structural composites, because of their limited density and their good adhesive and mechanical performances. Thanks to their chemical versatility and the wide variety of epoxy bases and/or chain extenders, they find application in various technological applications [1].

It has been recently demonstrated that the introduction of metal and carbon based nanofillers, such as metal nanopowders, carbon black (CB), carbon nanofibers (NFs), carbon nanotubes (CNTs), and graphite nanoplatelets (GnPs), can strongly modify the thermo-electrical behavior of the polymer matrices [2–4]. The influence of nanofiller addition on the electrical properties of polymer nanocomposites is usually explained considering the percolation theory [5]. Above a critical nanofiller concentration (i.e., the percolation threshold), a continuous network of conductive particles can be formed through the matrix, and the resistivity could therefore decrease by several orders of magnitude. For instance, the thermo-mechanical properties and the electrical resistivity variations under ramp and creep conditions of a nanofilled epoxy resin with different amounts of CB and NF was recently reported [6]. These nanomodified matrices can also be used to prepare glass fibers reinforced laminates whose deformation and

structural integrity can be monitored by electrical resistivity measurements [7].

Recently, various polymer matrices have been considered for the development of shape memory materials. These materials are endowed with the peculiar feature of “remembering” their original shape to which they return if an external stimulus (such as thermal, electrical, magnetic) is applied [8,9]. Shape memory alloys and shape memory polymers (SMPs) are currently among the most important types, and their efficacy is related to their final application [10]. They can be utilized in intelligent medical devices, smart textiles and apparels [11], high performance water–vapor permeability materials [12], heat shrinkable packages for electronics [13], self-deployable structures [14] and micro-systems [15]. As mentioned before, different external stimuli can be applied to SMPs to activate the shape recovery effect: heating [1,8,15,16], cooling [17], light [18,19], electric field [20–25], magnetic field [26–28], water [29], pH, ions or enzymes [30]. Recently, the demand to eliminate external heaters led to the development of novel electrically conductive SMPs filled with conductive nanofillers, such as CNTs [20,21], carbon particles [22,25], conductive fiber [23] and nickel zinc ferrite ferromagnetic particles.

For instance, the electro-activated shape memory behavior of a polycyclooctene (PCO)-based nanocomposite device was recently investigated by this group. CB and exfoliated GnPs (xGnP) were melt compounded at different concentrations with a crosslinked PCO matrix. A noticeable decrease of the electrical resistivity upon CB addition was detected, and nanocomposite with a CB amount of 4 wt% revealed also a noticeable heating capability by Joule effect above 100 V. The characterization of the prepared electro-active shape memory device demonstrated how it is possible to prepare a shape memory nanocomposite material able to completely recover its original shape after 100 s with a voltage of 90 V, retaining also the shape memory behavior after repeated thermal cycles [31,32]. Moreover, in a recent work of this group, silver nanoparticles were in-situ generated in an epoxy resin and various concentrations of CB and carbon NFs were added. CB was found to be more effective than NF in decreasing the electrical resistance of the matrix down to $10^3 \Omega\cdot\text{cm}$, and a rapid heating of the CB-filled samples upon voltage application was thus observed. The best electrical performances were obtained with a CB amount of 4 wt%, especially if silver nanoparticles were utilized. In fact, silver nanoparticles allowed a stabilization of the surface temperature of the samples for a prolonged voltage application time [33].

On the basis of the results obtained in this preliminary paper, the objective of the present work is to characterize the thermal, mechanical and electrical properties of new epoxy based nanocomposites nanomodified with in-situ reduced silver nanoparticles, in which both CB and NF were mixed in various ratios to reach a total filler amount of 4 wt%. The nanocomposite with optimized composition was then utilized to prepare and characterize an electro-active device with shape memory capability.

Correspondence to: A. Dorigato; e-mail: andrea.dorigato@unitn.it or A. Pegoretti; e-mail: alessandro.pegoretti@unitn.it
DOI 10.1002/pen.24985

Published online in Wiley Online Library (wileyonlinelibrary.com).

© 2018 Society of Plastics Engineers

EXPERIMENTAL

Materials

A DER 330 epoxy base (density = 1.16 g/ml, epoxy equivalent = 176–185 g/eq), provided by Dow Chemical Company (Midland, USA), and a Jeffamine D-400 aminic hardener (molecular weight = 430 Da, density = 0.972 g/ml, aminic equivalent = 115 g/eq), provided by Huntsman (Everberg, Belgium), were mixed to form the epoxy matrix.

The silver nanoparticles were generated in the epoxy hardener by the in-situ reduction of silver nitrate (AgNO_3 , Sigma Aldrich) [34]. The reaction solutions were prepared by dissolving 13.3 g of AgNO_3 in 100 g of hardener at 55°C. After 6 h, the obtained suspension manifested a strong UV-visible absorption band at 410 nm characteristic of Ag^0 (not reported here for the sake of brevity). TEM images demonstrated how the synthesized powder was constituted by nanostructured crystals with rather uniform spherical shape and diameter between 2 and 5 nm. Thermogravimetric measurements highlighted how the nanomodified hardener was characterized by an Ag amount of 8.6 wt% [33].

Ketjenblack EC600JD CB was provided by Akzo Nobel Chemicals Spa (Arese, Italy). It is constituted by aggregated primary particles with typical diameter of around 40 nm. The specific surface area (SSA) of CB nanoparticles was 1353 m^2/g [5], while helium pycnometry allowed to determine a density value of about 1.95 g/ml.

Vapour grown carbon NFs (1195JN) were purchased by NanoAmor Inc. (Houston). The producer's data sheet indicated a length of 5–40 μm , a core diameter of 0.5–10 nm, and an outside diameter of 240–500 nm. The SSA values of NF was 29 m^2/g , and their density was 1.78 g/ml. All materials were used without any preliminary treatment.

As the preparation of the samples is concerned, CB and NF were manually mixed at different relative concentrations with the epoxy base for 5 minutes. The mixture was then ultrasonicated for 10 min through a Hielscher sonicator at a specific power of 100 W/m^2 . The stoichiometric amount of hardener was then added to the mixture and manually mixed for 5 min. A base/hardener ratio of 100/63.9 was utilized in the case of neat epoxy, while for the Ag nanomodified epoxy a stoichiometric ratio of 100/70 was chosen, because of the presence of silver nanoparticles within the hardener. Considering that from TGA tests on the Ag nanomodified hardener an Ag content of 8.6 wt% was detected, the base/hardener ratio was adjusted in order to keep the same relative amount between the hardener and the epoxy base. The epoxy sample nanomodified with Ag nanoparticles had thus the 3.3 wt% of Ag, while in the nanofilled samples, in which the total nanofiller amount was kept constant at 4 wt%, the Ag concentration was slightly lower (i.e., 3.17 wt%).

After degassing, the compounded materials were poured in silicone moulds and cured for 2 h at 40°C + 3 h at 110°C + 2 h at 130°C. Samples with a mean thickness of 1.5 mm were thus prepared. Nanocomposites with a total filler nanofiller amount of 4 wt% were thus prepared by mixing together CB and NF at different relative concentrations. In order to evaluate the effect of the silver nanoparticles within the epoxy matrix, the same samples were prepared by using the Ag nanomodified matrix. Also neat epoxy and the epoxy sample nanomodified with Ag nanoparticles were prepared with the same procedure.

In the Results and Discussion section, neat epoxy and the Ag nanomodified matrix were denoted as EP and EP + Ag,

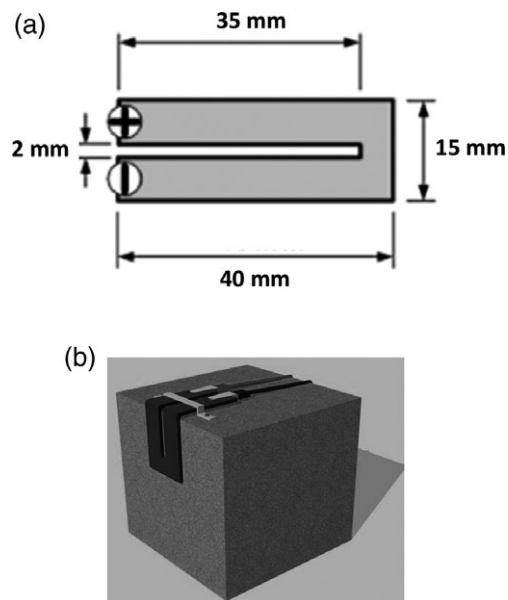


FIG. 1. (a) Representative image of the prepared shape memory device and (b) equipment utilized to evaluate the shape recovery degree of the electro-active device.

respectively. Nanofilled samples were designated indicating the nanofiller amount, the nanofiller type and the presence of Ag nanoparticles within the matrix. For instance, 2CB_2NF refers to the nanocomposite sample with a CB amount of 2 wt% and a NF concentration of 2 wt%, while Ag + 2CB_2NF indicates the same nanocomposite prepared by using the Ag nanomodified epoxy.

Testing Techniques

Field emission scanning electronic microscope (FESEM) images of the cryofractured surfaces of the nanocomposite samples were acquired through a Zeiss Supra 40 microscope, operating at an acceleration voltage of about 1 kV and a pressure of 10^{-6} Torr. Before the observations, the surfaces of the samples were metalized with a silver paste.

Differential scanning calorimetry (DSC) tests were carried out with a Mettler DSC30 machine (Schwerzenbach, Switzerland), in order to evaluate the effect of the nanofiller addition on the glass transition temperature (T_g) of the epoxy resin. A thermal ramp from -20 to 160°C , at a heating rate of $10^\circ\text{C}\cdot\text{min}^{-1}$ under a nitrogen flow of $100\text{ ml}\cdot\text{min}^{-1}$, was performed.

Flexural tests were carried out at 23°C and at relative humidity of 50% following the ASTM 790–10 standard through an Instron[®] 4502 testing machine (Norwood, MA). Rectangular samples, 2 mm thick and 5 mm wide, were utilized imposing a distance between the supports of 40 mm and a testing speed of 1.33 mm/min (maximum strain rate 0.01 min^{-1}). At least five specimens were tested for each sample. In this way, the elastic modulus (E) and the flexural stress at yield ($\sigma_{y,f}$) were determined.

Electrical bulk resistance measurements were carried out at 23°C and at relative humidity of 50% in direct current mode. A high resistance electrometer model 6517A 6 1/2-digit, provided by Keithley Instruments Inc. (Cleveland, OH), was utilized in 2-point test configuration. The sample surfaces in contact with the electrodes were painted with a silver coating, in order to decrease

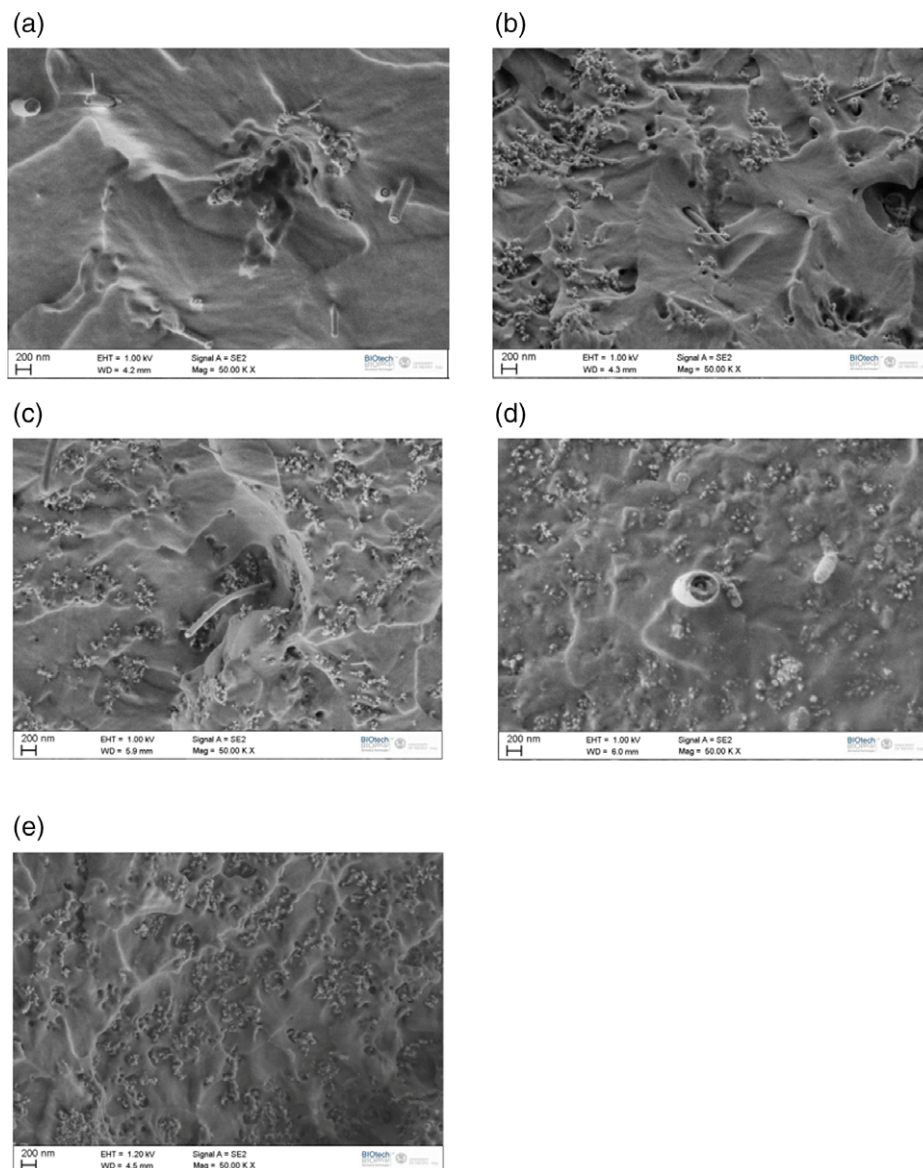


FIG. 2. FESEM images of the cryofracture surfaces of the prepared nanocomposites. (a) 4NF, (b) 1CB_3NF, (c) 2CB_2NF, (d) 3CB_1NF and (e) 4CB. [Color figure can be viewed at wileyonlinelibrary.com]

the contact resistance. The tests were performed on rectangular samples (cross section of 5×2 mm, length of 30 mm), and at least five specimens were tested for each composition. When the electrical resistance was lower than $10^5 \Omega$, measurements were carried out under an applied voltage of 10 V, and the resistance values were determined after 60 s, in order to minimize time-dependent effects. For electrical resistance between $10^5 \Omega$ and $10^{12} \Omega$, tests were carried out at 100 V. When the electrical resistance was higher than $10^{12} \Omega$, measurements were performed at an applied voltage of 1,000 V on square films (length of 95 mm and thickness of 2 mm). In this case, coaxial electrodes were used in order to minimize the amount of current flowing through the surface.

Due to the current flowing through the samples upon voltage application, an increase of the surface temperature by Joule effect was observed and measured. The same equipment and configuration used for electrical resistivity measurements was adopted, and voltage levels from 100 to 220 V were applied. The evolution of

the temperature reached by the electrical heating of the samples was detected through an Optris® LaserSight infrared digital thermometer, and one experimental point every 30 s was acquired.

The shape memory response of the Ag + 2CB_2NF nanocomposite was investigated. For this purpose, a rectangular strip cut from the prepared sheets having a length of 40 mm and a width of 15 mm was prepared. As described in Fig. 1a, a cavity 35 mm long and 2 mm wide was produced inside the sheet, and the electrodes were applied at the extremities of the device. The Joule heating effect produced by the current flow within the specimen was monitored through a Fluke Ti9 infrared thermocamera. The evolution of the surface temperature in different zones of this device was monitored. The investigation of the shape recovery degree of these devices was carried under the testing configuration reported in Fig. 1b. The device was fixed on a wood block and connected to the electrodes. The device was deformed until a programming angular position (θ_p) heating it through the application of a voltage of 100 V. After the complete cooling of the device

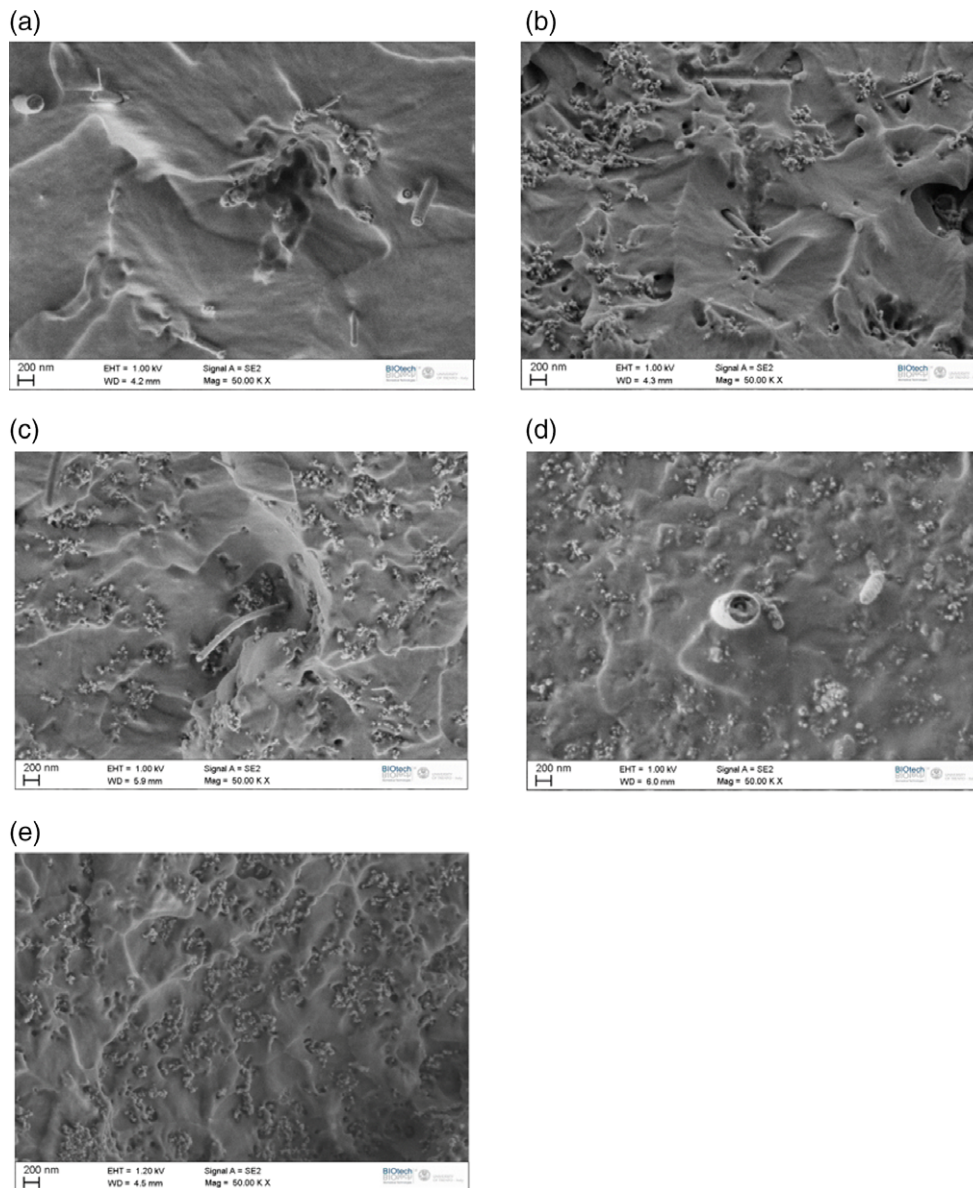


FIG. 3. FESEM images of the cryofracture surfaces of the prepared nanocomposites. (a) Ag + 4NF, (b) Ag + 1CB_3NF, (c) Ag + 2CB_2NF, (d) Ag + 3CB_1NF and (e) Ag + 4CB. [Color figure can be viewed at wileyonlinelibrary.com]

till room temperature, different voltage levels ranging from 70 to 150 V were applied. The degree of recovery (D.R.) of the shape was computed considering the angular position reached by the material at the different times (θ_r), as reported in Eq. 1:

$$D.R. = \left(\frac{\theta_r - \theta_f}{\theta_i - \theta_f} \right) \cdot 100 \quad (1)$$

where θ_i is the angular position of the undeformed device.

RESULTS AND DISCUSSION

Properties of Bulk Materials

It is well known that the thermal and the mechanical behavior of nanocomposite samples is directly influenced by the dispersion state of the nanofiller within the matrix. In Fig. 2a–e FESEM images of

the fracture surfaces of the prepared nanocomposites without Ag particles in the hardener are reported. As it is often reported in the scientific literature [6,7], the microstructure of 4CB nanocomposite is characterized by the presence of tiny and pale primary CB particles, homogeneously distributed within the epoxy matrix (Fig. 2e). As already observed in our previous paper [33], the aggregation tendency in CB filled nanocomposites increases with the nanofiller loading, because the mean interparticle distance diminishes and the probability of aggregation is therefore enhanced [35]. 4NF nanocomposite exhibits a more complex microstructure. Some cavities, most probably related to fiber-matrix debonding phenomena, can be detected on the fracture surface (Fig. 2a), and the mean diameter of the NFs is about 80 nm. In 1CB_3NF sample it is possible to notice that the dimension of CB aggregates is slightly reduced, while NF seem to be homogeneously distributed within the matrix, and some debonding is still visible (Fig. 2b). The same conclusions are valid also for the other samples (Fig. 2c and d).

In Fig. 3a–e FESEM micrographs of the prepared nanocomposites with Ag particles in the hardener are represented. Ag + 4CB composites are characterized by a morphology in which silver primary nanoparticles are homogeneously distributed within the matrix forming aggregates of four to five nanoparticles with a mean size of about 300 nm (Fig. 3e). Interestingly, the microstructure of Ag + 4NF sample is characterized by the presence of Ag aggregates localized near the NF or adhering on the NF surface (Fig. 3a). This microstructural feature could have an important role on the electrical conductivity of the resulting materials. The same microstructural features can be detected also for the other compositions (Fig. 3b–d), with Ag nanoparticles aggregates having a mean dimension of 75 nm and tending to preferentially adhere to NF surface.

In Table 1 glass transition temperature (T_g) values from DSC tests on neat epoxy and relative nanocomposites are summarized. In general it can be concluded that the T_g seems to be slightly reduced upon nanofiller addition, especially by adding CB nanoparticles. However, it is not possible to detect a clear trend of T_g with the relative CB/NF amount. A similar trend has been previously observed and reported by our group for various nanofilled thermosets [6,35–39], and it can be explained considering that the crosslinking process can be partially hindered at elevated filler concentrations. As already reported in our previous paper on similar epoxy systems [33], the observed T_g trend could be due to the occurrence of two concurrent phenomena: as the filler content increases the chain blocking mechanisms is more effective and leads to a slight T_g increase, while, at the same time, polymer-filler chemical interactions and the viscosity increase reduces the crosslinking degree of the matrix, thus reducing the T_g of the material. As recently reported by Liu et al. [40] on epoxy/alumina nanocomposites, the hardener molecules were unevenly distributed at a microscale, leading to a stoichiometric imbalance between epoxy components and reduced T_g values.

The elastic and yield properties of the prepared nanocomposites as a function of the CN/NF relative ratio are reported in Fig. 4a and b, respectively. As it often happens with epoxy systems having relatively low T_g (about 50°C in this case), the specimens do not show a brittle fracture under flexure, but the load reaches a maximum (i.e., flexural stress at yield), after which a plastic and irreversible deformation process without a clear failure occurs (representative stress–strain curves were not reported for the sake of brevity, but they can be found in [33]). For this reason, only

TABLE 1. Glass transition temperature from DSC tests on neat epoxy and relative nanocomposites

Samples	T_{g1} (°C)	T_{g2} (°C)
EP	49.3	49.0
4NF	45.3	48.1
1CB_3NF	46.7	49.7
2CB_2NF	45.9	49.6
3CB_1NF	42.3	42.7
4CB	43.0	43.4
EP + Ag	47.6	47.6
Ag + 4NF	45.4	44.1
Ag + 1CB_3NF	45.2	45.2
Ag + 2CB_2NF	45.0	45.2
Ag + 3CB_1NF	48.3	45.5
Ag + 4CB	42.7	42.6

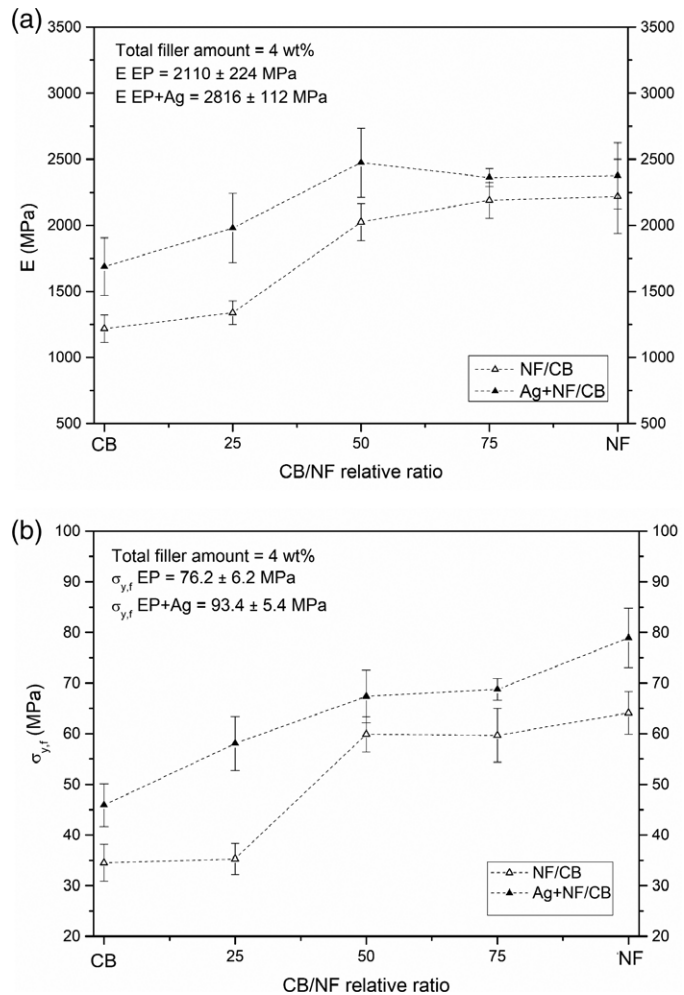


FIG. 4. Quasi-static tensile properties of the prepared nanocomposites. (a) Flexural modulus and (b) flexural stress at yield.

the flexural yield stress (and not the flexural stress at break) was reported. While both the elastic and the failure properties of the samples are only marginally affected by the NF addition within the material, the addition of CB markedly plasticizes the epoxy

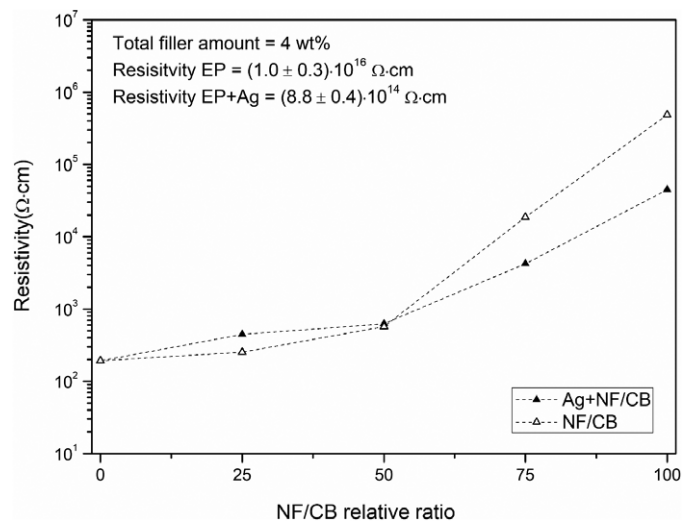


FIG. 5. Electrical resistivity of the prepared nanocomposites.

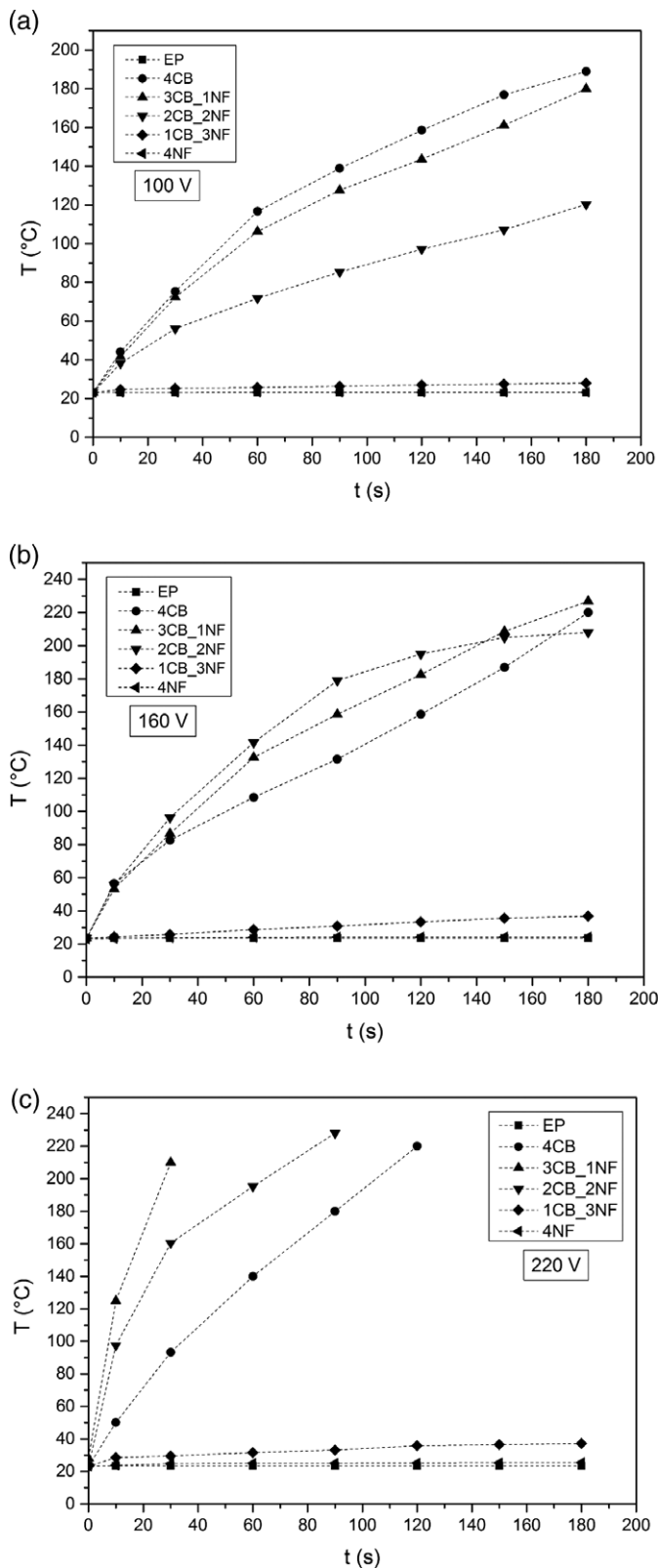


FIG. 6. Surface temperature evolution upon voltage application of the prepared nanocomposites (without Ag nanoparticles). Applied voltage of (a) 100 V, (b) 160 V and (c) 220 V.

matrix, similarly to what previously observed in epoxy/silica nanocomposites [41]. These results could be explained considering the lower T_g drop detected in DSC tests for NF-based

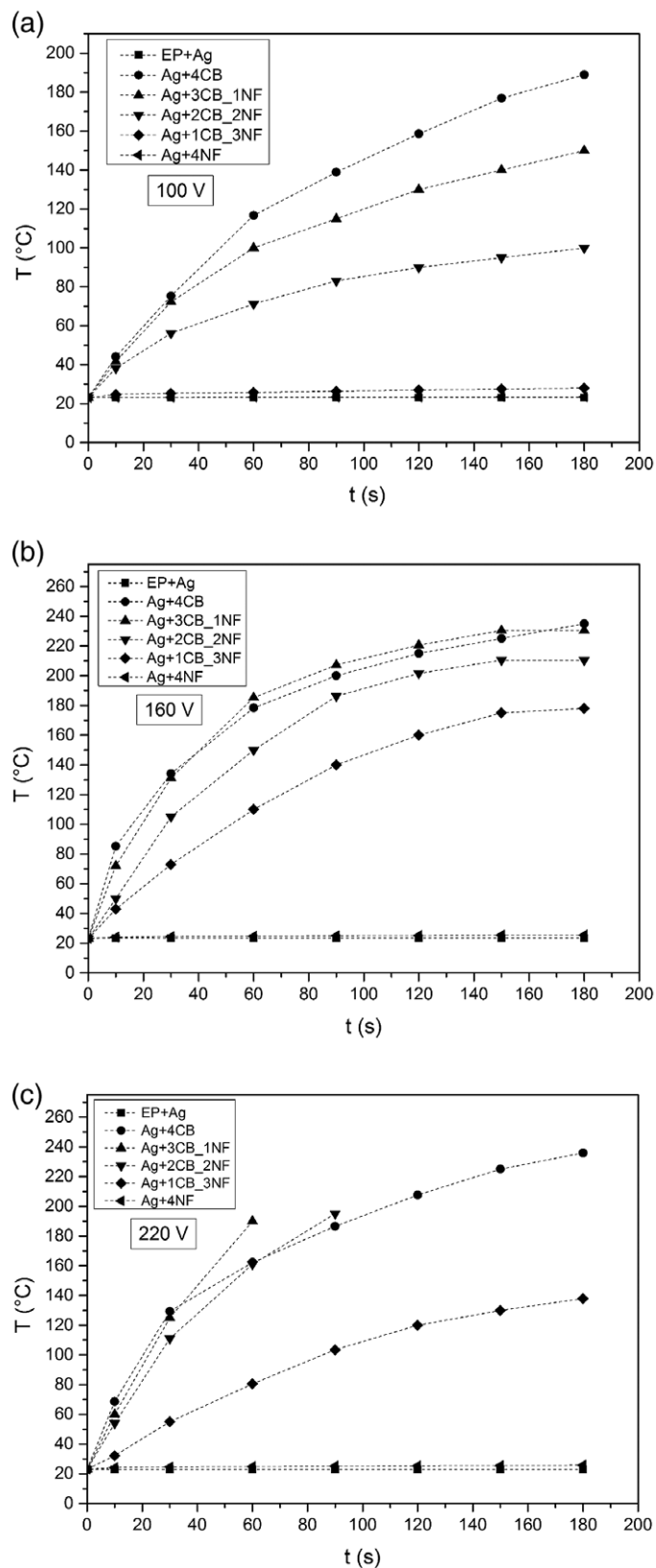


FIG. 7. Surface temperature upon voltage application of the prepared nanocomposites (with Ag nanoparticles). Applied voltage of (a) 100 V, (b) 160 V and (c) 220 V.

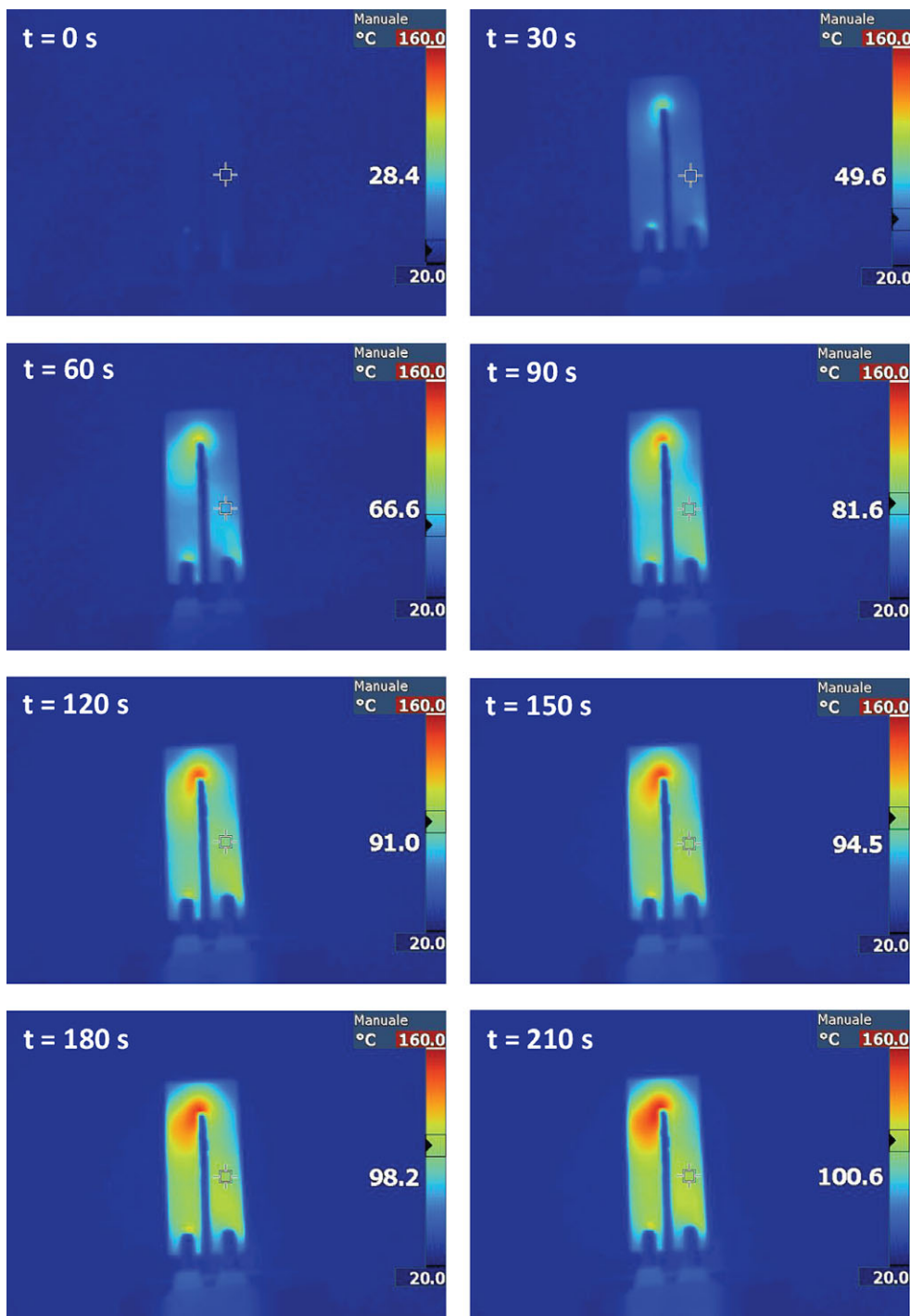


FIG. 8. Evolution of the surface temperature in the prepared electroactive device (applied voltage 220 V). [Color figure can be viewed at wileyonlinelibrary.com]

nanocomposites with respect to the CB filled ones. This difference in the effect on the T_g of the materials could be tentatively explained by considering the lower SSA of NF ($29 \text{ m}^2/\text{g}$) with respect to CB ($1,353 \text{ m}^2/\text{g}$) and, consequently, the different filler/matrix interactions. It is also interesting to note that the introduction of both NF and CB nanoparticles within the matrix promotes a synergistic effect, especially for CB/NF relative ratio of 50%, regardless to the presence of Ag nanoparticles in the hardener. As already observed in our previous paper [33], the introduction of silver nanoparticles systematically increases both the stiffness and

the yield resistance of the composites for all the tested compositions.

In Fig. 5 the trend of the electrical resistivity of the prepared nanocomposites as a function of the NF/CB relative ratio is reported. The electrical resistivity of the neat matrix is about $10^{16} \text{ } \Omega\text{-cm}$, in the typical range generally reported for epoxy resins [6], and the addition of Ag nanoparticles contributes to a slight resistivity reduction down to $9 \times 10^{14} \text{ } \Omega\text{-cm}$. This means that Ag addition at these concentrations does not allow to overcome the electrical percolation threshold in these systems. 4CB filled

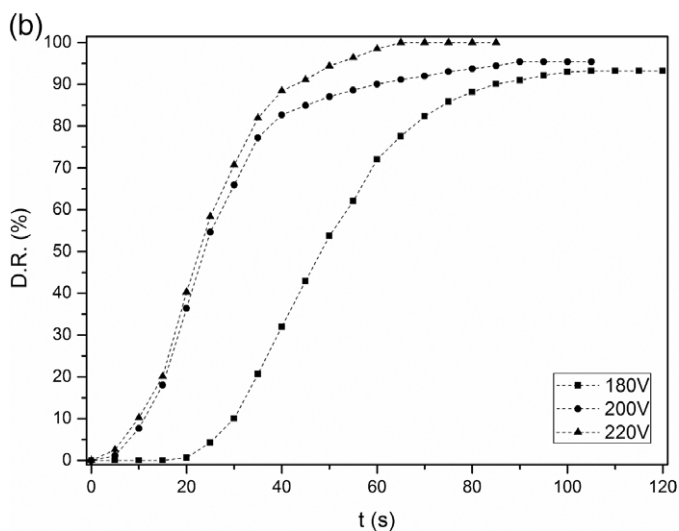
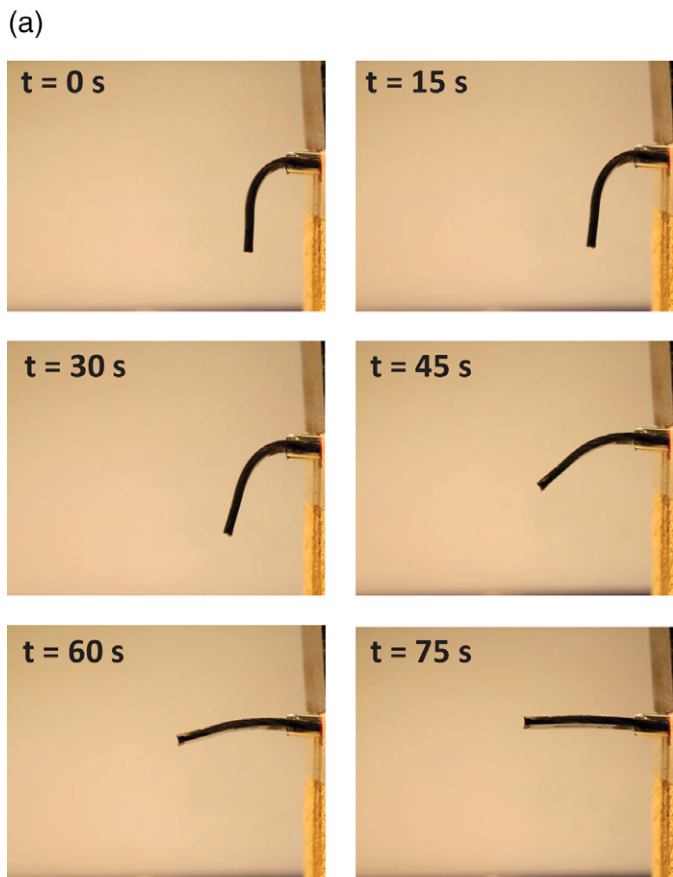


FIG. 9. (a) Shape recovery behavior of the prepared electroactive device (applied voltage 220 V) and (b) shape recovery degree of the prepared device at different voltage levels. [Color figure can be viewed at wileyonlinelibrary.com]

nanocomposite presents a resistivity of about $10^3 \Omega\text{-cm}$, and this value is not substantially influenced by the introduction of Ag nanoparticles. On the other hand, 4NF sample has a resistivity of $10^6 \Omega\text{-cm}$, but the introduction of Ag nanoparticles leads to a remarkable reduction of electrical resistivity up to $10^4 \Omega\text{-cm}$ after the percolation threshold. As already reported in our previous paper on these systems [33], the positive contribution played by

Ag nanoparticles on the conductivity of NF filled composites can be probably correlated to their peculiar morphological features. As reported in FESEM micrographs (Fig. 3), Ag aggregates are localized near NFs or directly adhere on NFs surface. Therefore, the formation of a conductive path is favored, with a consequent electrical resistivity drop. The resistivity of the 2CB + 2NF composite is about $6 \cdot 10^2 \Omega\text{-cm}$, very near to that of the 4CB sample that presents the lowest resistivity ($2 \cdot 10^2 \Omega\text{-cm}$). As already reported in our previous paper on PLA-based nanocomposites [42], this means that the combination of carbonaceous nanofillers with different morphology promotes a further decrease of the electrical resistivity, and the formation of a 3D conductive network within the matrix plays a key role in increasing electrical conductivity of the material.

Considering that the application of the investigated materials as electro active SMPs is strictly connected to their capability to reach the transition temperature (i.e., the glass transition temperature for epoxy systems) upon voltage application, surface temperature measurements at different voltages were performed. In Fig. 6a–c the time dependency of the surface temperature of the prepared nanocomposites without Ag nanoparticles in the hardener at three different voltage levels (100, 160, and 220 V) are reported. Except for the neat epoxy and the 4NF samples, it can be noticed that the surface temperature increases with the voltage application time, and the transition temperature (about 45°C) can be reached even at limited voltage (100 V). As it could be expected, the samples with the lower electrical resistivity present the higher heating rate, and the temperature reached by the material is proportional to the applied voltage. For instance, at an applied voltage of 100 V the 2CB_2NF sample is able to reach a surface temperature of 100°C in 120 s, while the same temperature can be reached in 30 and 10 s, applying respectively voltages of 160 and 220 V. It is interesting to note that Ag nanoparticles addition within the matrix is able to stabilize the temperature reached by the samples for long voltage application times (Fig. 7a–c). This feature is probably related to the high heat dissipation capability of Ag nanoparticles within the matrix. Considering that the electrical conductivity of CB nanocomposites is not substantially affected by the presence of silver within the matrix, this peculiar feature can be related to the higher heat dissipation capability of the composites in the presence of metallic nanoparticles. This aspect is very important to prevent the overheating and thus the thermal degradation of the material at elevated voltages.

Electroactive Shape Memory Behavior

On the basis of the performed characterization activity, it could be concluded that the Ag + 2CB_2NF composite is able to provide the best balance of the properties. In fact, with this composition it is possible to achieve a low resistivity value, retaining the mechanical properties of the pristine matrix. This formulation was therefore selected to prepare the specimens to test the electroactive shape memory behavior. In Fig. 8, the evolution of the surface temperatures of the prepared shape memory device at an applied voltage of 220 V in the terminal and in the lateral zones is shown. It is interesting to note how an inhomogeneous temperature distribution is obtained, and that the maximum temperature can be reached in the terminal region of the device. It is probable that in this point a geometrical concentration of the current flow occurs, thus increasing the local temperature of the material.

Therefore, similar voltage application times induce a higher temperature in the terminal zone compared with the lateral section of the device. In any case, after 60 s all the regions of the device reach a temperature higher than that required for the activation of the shape memory effect (i.e., the T_g of the epoxy resin).

The shape memory behavior of the electroactive SM device was finally evaluated. In Fig. 9a, shape recovery at different times with an applied voltage of 220 V is shown, while in Fig. 9b D.R. values at different voltage levels is reported. It is interesting to note that under an applied voltage of 220 V the specimen is able to reach a D.R. of 50% in 20 s, while the original shape can be recovered in about 60 s. Moreover, the tested specimen is able to almost completely recovery its original shape (i.e., D.R. > 90%) in the whole range of considered voltages. As it could be expected, the shape recovery speed is proportional to the applied voltage. It was therefore demonstrated the possibility to prepare an electro-active shape memory material able to recover its original shape in a short time, applying voltage levels lower than 220 V.

CONCLUSIONS

In this work, the electroactive shape memory behavior of a nanocomposite shape memory material was investigated. An epoxy resin was nanomodified with in-situ generated silver nanoparticles and filled with both CB and NF at different relative ratios, keeping a constant filler amount of 4 wt%, and the resulting materials were thermoelectrically characterized.

DSC tests revealed how the addition of both CB and NF led to a slight decrease of the glass transition temperature of the material, while FESEM micrographs evidenced how the morphology is strongly dependent by the CB/NF relative ratio and by the presence of Ag nanoparticles. Because of the T_g drop due to nanofiller addition, both flexural modulus and stress at yield were decreased with respect to the neat resin, especially at elevated CB concentrations, while the introduction of Ag nanoparticles promoted an increase of the flexural properties. An interesting synergistic effect was observed both in the mechanical and in electrical properties for the samples at CF/NF ratio of 50%. For this composition, an interesting decrease of the electrical resistivity up to $10^2 \Omega\cdot\text{cm}$, coupled with a noticeable heating capability through Joule effect, was detected.

The characterization of the electroactive shape memory response of this composition highlighted how an almost complete shape recovery could be obtained after 60 s under an applied voltage of 220 V.

ACKNOWLEDGMENTS

Prof. Federica Bondioli (University of Parma (Italy), Department of Engineering and Architecture) is gratefully acknowledged for the kind provision of silver nanoparticles. Dr Giovanni Giusti is gratefully acknowledged for his support to the experimental work.

REFERENCES

1. C. Liu, H. Qin, and P.T. Mather, *Journal of Materials Chemistry*, **17**(16), 1543 (2007).
2. Z.J. Fan, C. Zheng, T. Wei, Y.C. Zhang, and G.L. Luo, *Polymer Engineering and Science*, **49**(10), 2041 (2009).
3. J. Li, P.S. Wong, and J.K. Kim, *Materials Science and Engineering A*, **483–484**(SI), 660 (2008).
4. J. Sumfleth, S.T. Buschhorn, and K. Schulte, *Journal of Materials Science*, **46**(3), 659 (2010).
5. M. Traina, A. Pegoretti, and A. Penati, *Journal of Applied Polymer Science*, **106**(3), 2065 (2007).
6. D. Pedrazzoli, A. Dorigato, and A. Pegoretti, *Journal of Nanoscience and Nanotechnology*, **12**(5), 4093 (2012).
7. D. Pedrazzoli, A. Dorigato, and A. Pegoretti, *Composites Part A - Applied Science and Manufacturing*, **43**(8), 1285 (2012).
8. A. Lendlein and S. Kelch, *Angewandte Chemie International Edition*, **41**, 2034 (2002).
9. R. Bogue, *Assembly Automation*, **29**(3), 214 (2009).
10. L. Sun, W.M. Huang, Z. Ding, Y. Zhao, C.C. Wang, H. Purnawali, and C. Tang, *Materials and Design*, **33**, 577 (2012).
11. Q.H. Meng, J.L. Hu, Y. Zhu, J. Lu, and Y. Liu, *Smart Materials and Structures*, **16**, 1192 (2007), 1197.
12. S. Mondal, J.L. Hu, and Y. Zhu, *Journal of Membrane Science* **280**, 427 (2006), , 432.
13. A. Charlesby, *Atomic radiation and polymers*, Pergamon Press, (1960).
14. B.K. Kim, S.Y. Lee, and M. Xu, *Polymer*, **37**, 5781 (1996).
15. K. Gall, M.L. Dunn, Y. Liu, D. Finch, M. Lake, and N. A. Munshi, *Acta Materialia*, **50**, 5115 (2002).
16. J.L. Hu, F.L. Ji, and Y.W. Wong, *Polymer International*, **54**(3), 600 (2005).
17. C.C. Wang, W.M. Huang, Z. Ding, Y. Zhao, and H. Purnawali, *Composites Science and Technology*, **72**, 1178 (2012).
18. A. Lendlein, H.Y. Jiang, O. Junger, and R. Langer, *Nature*, **434**, 879 (2005).
19. H. Jiang, S. Kelch, and A. Lendlein, *Advanced Materials*, **18**(11), 1471 (2006).
20. J.W. Cho, J.W. Kim, Y.C. Jung, and N.S. Goo, *Macromolecular Rapid Communication*, **26**(5), 412 (2005).
21. I.H. Paik, N.S. Goo, Y.C. Jung, and J.W. Cho, *Smart Materials and Structures*, **15**(5), 1476 (2006).
22. B. Yang, W.M. Huang, C. Li, L. Li, and J.H. Chor, *Scripta Materialia*, **53**(1), 105 (2005).
23. J.S. Leng, H.B. Lv, and Y.J. Liu, *Applied Physics Letters*, **91** (2007).
24. A.M. Schmidt, *Macromolecular Rapid Communication*, **27**(14), 1168 (2006).
25. H. Koerner, G. Price, N. Pearce, M. Alexander, and R.A. Vaia, *Natural Materials*, **3**(2), 115 (2004).
26. J.S. Leng, X. Lan, Y.J. Liu, S.Y. Du, W.M. Huang, N. Liu, S. J. Phee, and Q. Yuan, *Applied Physics Letters*, **92**, 014104 (2008).
27. J.S. Leng, W.M. Huang, X. Lan, and Y.J. Liu, *Applied Physics Letters*, **92**, 204101 (2008).
28. U. Narendra Kumar, K. Kratz, M. Behl, and L. A, *Express Polymer Letters*, **6**(1), 26 (2012).
29. K. Fan, W.M. Huang, C.C. Wang, Z. Ding, Y. Zhao, H. Purnawali, K.C. Liew, and L.X. Zheng, *Express Polymer Letters*, **5**(5), 409 (2011).
30. M. Behl and A. Lendlein, *Materials Today*, **10**(4), 20 (2007).
31. A. Dorigato, M. Sebastiani, A. Pegoretti, and L. Fambri, *Journal of Polymers and the Environment*, **20**, 713 (2012).
32. A. Dorigato and A. Pegoretti, *Polymer Engineering and Science*, **57**, 537 (2017).
33. A. Dorigato, G. Giusti, F. Bondioli, and A. Pegoretti, *Express Polymer Letters*, **7**(8), 673 (2013).
34. Y. Young, S. Matsubara, L. Xiong, T. Hayakawa, and M. Nogami, *Journal of Physical Chemistry C*, **111**, 9095 (2007).

35. M. Buccella, A. Dorigato, E. Pasqualini, M. Caldara, and L. Fambri, *Journal of Polymer Research*, **19**(9935) (2012).
36. A. Dorigato and A. Pegoretti, *Journal of Nanoparticle Research*, **13**(6), 2429 (2011).
37. A. Dorigato, A. Pegoretti, and P. A., *Journal of Reinforced Plastics and Composites*, **30**(4), 325 (2011).
38. A. Dorigato, A. Pegoretti, F. Bondioli, and M. Messori, *Composite Interfaces*, **17**(9), 873 (2010).
39. A. Pegoretti, A. Dorigato, M. Brugnara, and A. Penati, *European Polymer Journal*, **44**(6), 1662 (2008).
40. G. Liu, H. Zhang, D. Zhang, H. Zhang, Z. Zhang, X. An, and X. Yi, *Journal of Materials Science*, **47**, 6891 (2012).
41. M. Preghenella, A. Pegoretti, and C. Migliaresi, *Polymer*, **46**(26), 12065 (2005).
42. M. Tait, A. Pegoretti, A. Dorigato, and K. Kaladzidou, *Carbon*, **49**, 4280 (2011).